Engineering xxx (xxxx) xxx

Contents lists available at ScienceDirect

Engineering

journal homepage: www.elsevier.com/locate/eng

Research
Environmental Engineering—Review

Advancing Indoor Air Purification by Mass Transfer Enhancement: Bridging the Gap Between High-Performance Materials and Technologies

Enze Tian [b], Qiwei Chen [c,d], Yilun Gao [c], Zhuo Chen [e], Yan Wang [c], Jinhan Mo [a,c,f,g,*]

[a] College of Civil and Transportation Engineering, Shenzhen University, Shenzhen 518060, China
[b] Songshan Lake Materials Laboratory, Dongguan 523808, China
[c] Beijing Key Laboratory of Indoor Air Quality Evaluation and Control, Department of Building Science, Tsinghua University, Beijing 100084, China
[d] China Construction First Group Construction & Development Co., Ltd., Beijing 100102, China
[e] Department of Civil and Environmental Engineering, The Hong Kong Polytechnic University, Hong Kong, China
[f] State Key Laboratory of Intelligent Geotechnics and Tunnelling, Shenzhen University, Shenzhen 518060, China
[g] State Key Laboratory of Subtropical Building and Urban Science, Shenzhen University, Shenzhen 518060, China

ARTICLE INFO

Article history:
Received 5 June 2024
Revised 25 May 2025
Accepted 2 July 2025

Keywords:
Mass transfer
Air cleaning
Particulate matter
Formaldehyde
Indoor air quality

ABSTRACT

Indoor air purification, as a typical gas–solid interface process, involves the transfer of airborne pollutants to purification material surfaces through mass transfer, enabling their removal. While research on indoor air purification materials has expanded remarkably, studies on enhancing mass transfer have been relatively limited. In this work, we proposed a new concept of "integration of mass transfer and material regulation," aiming to provide a design methodology for indoor air purification. Taking solid-phase particulate matter (PM) filtration and gas-phase pollutant adsorption as examples, we summarized the novel approach that shifts from passive material usage to active control of mass transfer through multiscale (milli–micro–nano) and multifield (mass–flow–force). For PM removal, the external electric force can enhance the migration velocity of PM towards the fiber approximately fivefold, resulting in 1–3 orders of magnitude higher comprehensive quality factor than commercial filters, considering filtration efficiency, pressure drop, and energy consumption. For gas removal, the hierarchical structure can increase the gas–solid contact area by 58%, resulting in a 37% improvement in single-pass removal efficiency and a 152% enhancement in dynamic adsorption capacity. We bridge the gap between high-performance materials and technologies by providing a design methodology for controlling surface forces and structures to improve mass transfer.

1. Introduction

Indoor air pollution, including both airborne particulate matter (PM) in the solid phase and chemical pollutants in the gas phase, poses paramount global environmental risks for human health [1] and high-end manufacturing industries [2]. Extensive research has established that prolonged or accidental exposure to indoor air pollutants can cause respiratory ailments [3], tumorous diseases [4], cognitive impairments [5], and even death [6]. In 2020, indoor air pollution caused approximately 3.2 million deaths globally, comparable to the 3.5 million deaths caused by outdoor pollution [7]. Moreover, cleanroom airborne contamination control is crucial to product quality and individual safety in high-tech industries such as semiconductors and medicine [8,9].

Healthy buildings and cleanrooms must safeguard people and products from external atmospheric pollution while mitigating internal contamination. Indoor air purification plays a crucial role in achieving this goal. Two air purifiers equipped with high-efficiency particulate air (HEPA) filters can potentially reduce airborne PM exposure by 65% for three individuals in a 54 m^2 room [10]. Combining ventilation with air purification in a gym could reduce the PM concentration to 5%–10% of baseline levels, significantly reducing the risk of airborne disease transmission [11]. Clean rooms for semiconductor manufacture require HEPA filters for product yield. The cascaded filtration in two 100 class clean rooms reduced PM concentrations with diameters larger than 0.3 μm to <1000 count·m^{-3} [12]. It is worth noting that indoor air purification holds profound strategic implications for human

* Corresponding author.
E-mail address: mojinhan@szu.edu.cn (J. Mo).

https://doi.org/10.1016/j.eng.2025.07.003

Please cite this article as: E. Tian, Q. Chen, Y. Gao et al., Advancing Indoor Air Purification by Mass Transfer Enhancement: Bridging the Gap Between High-Performance Materials and Technologies, Engineering, https://doi.org/10.1016/j.eng.2025.07.003

habitation in deep-sea, underground, and outer space environments, as it directly impacts the duration of human stays in such settings.

However, indoor air purification not only plays a crucial role in safeguarding but also in reducing energy costs and greenhouse gas emissions in various inhabited spaces [7]. Due to the low concentration of indoor air pollutants compared to industrial pollutants, conventional purification technologies require a strategic reduction in the gap between the pollutants and the purification medium to ensure efficient and rapid pollutant removal. However, tightly compacted purification medium blocks fluid dynamics, resulting in high wind-pressure drop over the medium and high fan energy consumption. Increased wind-pressure drop or decreased efficiency during operation can also shorten the filters' service life. Public buildings in China consume 20%–30% of their total power for ventilation and filtration, resulting in an annual power consumption of over 200 billion kW·h. Cleanrooms, with air exchange rates 4–80 times higher than public buildings [13], have even higher energy consumption for ventilation and filtration, leading to significant expenses in industrial production.

In brief, traditional high-efficiency purification methods often struggle to achieve high efficiency and low air resistance due to the necessity for greater medium density, leading to high air resistance. Achieving high efficiency while maintaining low air resistance is considered the "holy grail" challenge in purification research [14]. This challenge stems primarily from the lack of a comprehensive approach that integrates mass transfer enhancement with material regulation for indoor air purification. Despite recent advances in air purification materials such as nanofibers [15], metal–organic–framework (MOF) [16], and two-dimensional materials [17], the challenge lies in the mismatch between material performance and purification efficiency when ignoring mass transfer enhancement.

To provide a design methodology for indoor air purification engineering, we introduce the concept of "integration of mass transfer and material regulation" in this work. Section 2 demonstrates the principle of increasing air purification efficiency while saving energy. Sections 3 and 4 offer principle-based indoor air purification technologies with low energy consumption, high efficiency, and long service life, using particulate filtration and chemical pollutant adsorption as examples. Section 5 summarizes the main viewpoints and promotes next-generation indoor air purification technology design.

2. Increasing efficiency and reducing energy consumption of air purification

The clean air delivery rate (CADR) is an important parameter that characterizes an air cleaner's indoor air purification ability. It quantifies the rate at which an air cleaner can generate clean air over a specific unit of time, which Eq. (1) determines [18]:

$$\mathrm{CADR} = G \cdot \left(1 - \mathrm{e}^{-\mathrm{NTU_m}}\right) \tag{1}$$

where G is the airflow rate, $\mathrm{m^3 \cdot s^{-1}}$, which contributes most importantly to CADR [19]; $\mathrm{NTU_m}$ is the number of the mass transfer unit and is further determined by three dimensionless parameters, as shown in Eq. (2) [18]:

$$\mathrm{NTU_m} = A^* \cdot \mathrm{St_m} \cdot \eta \tag{2}$$

where A^* is the dimensionless characteristic surface area for mass transfer (the ratio of the purification area of the targeted pollutants to the cross-sectional area of the air purification module); $\mathrm{St_m}$ is the Stanton Number for mass transfer, which characterizes the interfacial mass transfer and is between 0 and 1; η is a dimensionless coefficient related to material properties, which describes the material characteristic and is also between 0 and 1. The three parameters have equal weights in determining $\mathrm{NTU_m}$ and further CADR. It means when the breakthrough of material performance is hard to realize, the performance of an air cleaner can be effectively improved by optimizing the structure of the cleaner (e.g., enhancing the contact area of airborne pollutants to the materials) or by strengthening the interface mass transfer of airborne pollutant to the materials (Fig. 1).

For the structural design of air cleaners, the contact area of airborne pollutants to the materials, that is, the mass transfer area, should be increased. Taking gas-phase air cleaning as an example, inspired by the heat transfer fins, the sub-milli-sized fin structure could be considered in fabricating adsorption components [20]. Besides, Chen et al. [21,22] reported that the net-like honeycomb structure can also be applied as it has a high specific surface area.

Eq. (3) can be used to guide the enhancement of interfacial mass transfer:

$$\varphi = h_\mathrm{m} \cdot \left(C_\infty - C_\mathrm{interface}\right) \tag{3}$$

where ϕ is the mass transfer flux per unit area, $\mathrm{mg \cdot m^{-2} \cdot s^{-1}}$; h_m is the convective mass transfer coefficient, $\mathrm{m \cdot s^{-1}}$; C_∞ is the pollutant concentration in the inflow, $\mathrm{mg \cdot m^{-3}}$; $C_\mathrm{interface}$ is the pollutant concentration on the interface of the airborne pollutant to the materials. Eq. (3) provides insight into the parameters determining ϕ, including h_m and the difference between C_∞ and $C_\mathrm{interface}$.

Among them, h_m can be realized by enhancing the turbulence of the flow, which can be realized by building some surface microstructures [23]. For particulate filtration, h_m depends on the external field forces to which the particles are subjected, such as gravity, centrifugal force, electrostatic force, thermophoretic force, and so forth. The greater the external field force exerted toward the fibers, the faster the PM's transfer velocity and the greater the h_m. For gas purification, the interfacial mass transfer includes two steps: external mass transfer from the airflow to the mass transfer boundary layer and internal mass transfer from the boundary layer into the inner material. However, for most adsorption mass transfer processes, the internal mass transfer is the primary resistance limiting the whole process. Maintaining a large concentration gradient is essential for a sufficient external mass transfer driving force. It requires keeping the $C_\mathrm{interface}$ at a low level compared to C_∞ over time, which necessitates the rapid internal diffusion of adsorbed gas from the adsorbent surface. The goal is to ensure that the adsorbate is uniformly distributed throughout the material instead of accumulating on the surface. Therefore, enhancing the diffusion mass transfer inside the material is paramount. Since adsorbents are generally porous materials, optimizing the porosity and the pore size distribution is usually the most effective method [24,25]. Furthermore, an interconnected pore structure is crucial for facilitating the diffusion transfer of gas molecules within the material [26,27].

3. Upgrade indoor PM filtration performance with electrostatic force

Indoor PM pollution has gained significant attention due to respiratory epidemics such as corona virus disease 2019. Efficient PM (including bioaerosol) removal technologies are essential for ensuring clean and healthy built environments [28]. Filtration is frequently used among these technologies because of its low cost, easy operation, and high efficiency. Synthetic polymers such as polyethylene and polypropylene are often used in commercial air filters because of their affordability and adaptability. Electrospinning methods have been developed to generate nanofibers from diverse synthetic polymers, improving filtering efficacy and reducing the wind-pressure drop. Natural polymers, including cellulose

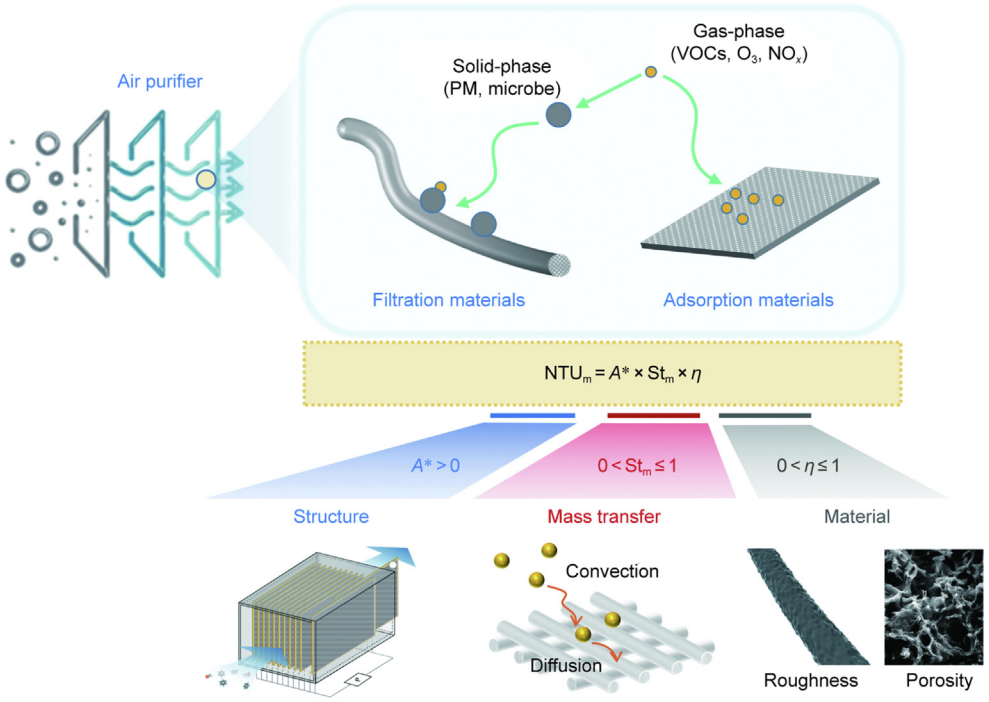

Fig. 1. Improving air cleaning performance through structural modifications, interfacial mass transfer enhancement, and material property optimization. VOCs: volatile organic compounds.

and chitosan, have demonstrated commendable filtration efficiency and recyclability for their superior biocompatibility and biodegradability. Besides, nanomaterials, including MOF, carbon nanotubes, and graphene oxide, have been deposited onto fiber substrates for superior mechanical properties, hydrophobicity, and surface area. For applications in extreme conditions, inorganic and metallic fibers, including SiO_2, Al_2O_3, Si_3N_4, and SiC, have been developed for PM filtration at elevated temperatures [29].

These innovative materials allow the creation of diverse air filtration products, such as face masks, smart windows, indoor air purifiers, bag filters, and gasoline filters, enhancing air quality and safeguarding human health. However, current filter materials often struggle to balance filtration efficiency, wind-pressure drop, and PM holding capacity. Many studies [30,31] have demonstrated that electrostatic assistance enhances filtration efficiency and reduces the wind-pressure drop. The following section reviews current advances in the mechanism, device build-up, material preparation, and electrostatically assisted air filtration performance for indoor PM removal. The goal is to improve the fundamental understanding of high-performance PM filtration from the perspective of mass transfer enhancement by electrostatic force.

3.1. Motivation for coupling PM filtration with electrostatic force

In a typical indoor PM filtration process, fibers capture PM in the air flow while air molecules penetrate them. Air molecules are expected to pass through the fibers with minimal resistance to maintain an extremely low wind-pressure drop, while all airborne PM is expected to be removed for 100% filtration efficiency. The pressure drop of the fibrous materials depends on the filter's intrinsic properties and the airflow characteristics. The random distribution of fibers within the filtration material poses challenges in accurately calculating the pressure drop. Despite this, the low-pressure drop is typical of fibrous materials with large pores, high porosity, and thin thickness. However, these preferable parameters for low-pressure-drop fibrous material can also lead to low filtration efficiency, as indicated by Eqs. (4) and (5) [32]:

$$\Delta p = 64\mu v_{\text{air}} \frac{\alpha^{1.5} \cdot (1 + 56\alpha^3)L}{d_{\text{f}}^2} \tag{4}$$

$$\eta_f = 1 - \exp\left(\frac{4\alpha L}{\pi(\alpha - 1)d_f}\eta_s\right) \tag{5}$$

where Δp refers to the pressure drop of a porous filter (Pa); μ is air viscosity (Pa·s); v_{air} indicates the face air velocity over the filter ($m \cdot s^{-1}$); α represents the fiber volume percentage in the filter; L represents the filter thickness (m); d_{f} refers to the fiber diameter (m); η_{f} refers to the filtration efficiency of a fibrous filter made up of cylinder fibers of the same size, placed perpendicular to the airflow and packed evenly; and η_{s} refers to the filtration efficiency of a single cylinder fiber.

To achieve minimal pressure drop while enhancing the filtration efficiency of the fibrous filter, it is crucial to improve η_{s}, as indicated by Eqs. (4) and (5). The contact probability between a particle and a fiber positively correlates with the PM migration velocity towards the fiber and then determines η_{s}. The PM migration velocity is influenced by various external fields, including electric, magnetic, temperature, and centrifugal force fields, which drive the mass transfer process of PM onto the fiber surface. For $PM_{2.5}$ (particulate matter with aerodynamic diameters less than 2.5 μm), which is of significant concern for indoor air quality, electrostatic force plays a crucial role in enhancing the particle migration velocity while minimizing energy dissipation (Fig. 2(a)) [33].

Numerous researchers have utilized electrostatic forces to enhance the mass transfer of PM onto fibers (Fig. 3 [34–38]). Typical technologies include electret filters [39], electrospun nanofiber filters [15], tribo-charge enhanced filters [34], electric field induced-charge enhanced filters [35], and ion-assisted filters [36]. These approaches for charging either PM or fibers offer simple construction and convenient replacement. However, when only PM or fibers are charged, the electrostatic force on the PM is referred to

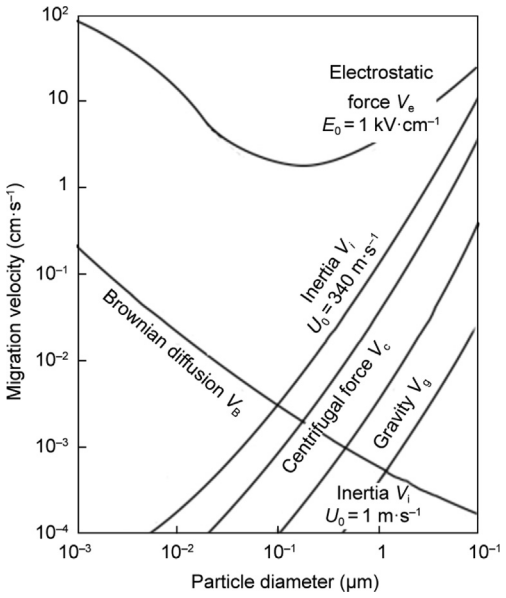

Fig. 2. (a) PM migration velocity encouraged by different effects [33]. v_e, v_B, v_i, v_c and v_g: particle migration velocity caused by electrostatic force, Brownian diffusion, inertia, centrifugal force, and gravity, respectively; E_0: electric field intensity; U_0: air velocity. Reproduced from Ref. [33] with permission.

as dielectrophoretic force and image force, which are comparatively weaker than the Coulomb force generated when both PM and fibers are charged [40].

To further enhance the mass transfer of PM towards fibers, some researchers simultaneously charge PM and fibers with opposite charges, remarkably improving filtration efficiency. Microscopic charge-coupled device (CCD) cameras have been employed to observe the enhanced PM migration velocity boosted by an electric field [41]. As a result of the application of an electrostatic field, the migration velocity of charged particles significantly increases when they move toward the polarized fiber surface. When located at a distance of about 6 μm from the fiber surface, the migration velocity experiences an approximately fivefold increase compared to the scenario without an electric field (Fig. 4 [41]).

3.2. System of the two-stage electrostatically assisted air (EAA) filtration process

Researchers have proposed various approaches for simultaneously charging PM and fibers [37,38]. In these approaches, particles acquire charge through ion generators, corona discharge, and plasma discharge. Fibers can be classified into two types: conductive fibers and dielectric fibers. Conductive fibers acquire charge by being connected to a power supply, such as a battery [42] or a nanogenerator [43]. Dielectric fibers acquire a one-off charge through electret or electrospinning techniques. Alternatively, continuous polarization in an electric field can obtain a long-lasting induced charge. Charge decay is a concerning issue in one-off charging and ion generators [44], and plasma discharge and continuously charging conductive fibers have drawbacks of high energy consumption and cost [31]. Consequently, simultaneously charging PM by corona discharge and charging dielectric fibers by continuous polarization, namely two-stage EAA filtration [45], has emerged as a promising electrostatic-force enhanced filtration technology with potential applications.

For a charged PM and a dielectric cylindrical fiber in an external electric field for polarization, the radial Coulomb force F_E (N) between them can be described by Eq. (6) [32]:

$$F_E = q_p E_\infty \left[1 + \left(\frac{\varepsilon_f - 1}{\varepsilon_f + 1}\right)\frac{d_f^2}{4r^2}\right] \quad (6)$$

where q_p (C) is the charge on the particle; E_∞ (V·m^{-1}) refers to the external electric field intensity perpendicular to the fiber's center line and passes through the center of the particle; ε_f is the relative dielectric constant of the fiber; d_f (m) is the fiber diameter; r (m) is the distance between the particle and the fiber.

According to Eq. (6), the migration process of charged PM to fibers can be categorized into three regions based on r, namely the accelerating region, the capturing region, and the adhesion region (Fig. 5(a)) [46]. In the accelerating region ($r >> d_f$), the fiber-related parameters (including ε_f, d_f, and r) exhibit minimal influence on F_E, while q_p and E_∞ primarily determine F_E. PM accelerates in the air flow due to the near-consistent F_E until reaching a force equilibrium. In the capture region ($r \sim d_f$), the induced electric field around the dielectric fibers significantly influences F_E. The shorter r/d_f, the larger ε_f, the stronger the F_E. As a result, the PM experiences an increasing F_E as they migrate towards the fibers until being captured on the fiber surfaces. In the adhesion region, where the PM is trapped by the fiber ($r \approx d_p/2 + d_f/2$), the interaction between PM and fibers involves F_E and van der Waals forces. Depending on the surface energy and roughness of the fiber, the van der Waals forces can be significantly stronger than F_E, deciding whether the captured PM would be released.

A fundamental method to construct an EAA filtration device involves creating two sets of charging electrodes (Fig. 5(b) [45]). The particle charging electrodes consist of a (nearly) flat grounding electrode and an electrode with a narrow curvature radius connected to a high-voltage power supply. The two types of electrodes create an uneven electric field that enables corona discharge for particle charging. On the other hand, the fiber charging electrodes consist of two perforated plates or nets that are parallel to each other, with one connected to high voltage and the other to the ground. This electrode pair ensures a uniform electric field over the filter material between them, effectively charging the filter through polarization [45].

In cases where a more compact device is desired, the two high-voltage electrodes can be merged into one [50]. However, there would be a significant coupling between the discharge and polarization zones, which may hinder optimal overall filtration performance. When the device's size is not concerned, an additional grounding electrode can be installed between the two high-voltage electrodes [46]. To minimize interference between the discharge and polarization zones, the distances between the additional grounding electrode and the two high-voltage electrodes should not be shorter than the distances between the two high-voltage electrodes and their corresponding grounding electrodes.

Furthermore, the PM charging and filter polarizing structural units can be improved. For example, W-shaped polarization electrodes were designed to expand the filtration area, reducing air filtration velocity and air resistance and enhancing filtration efficiency and dust-holding capacity (Fig. 5(c)) [47]. A two-stage cascaded corona charger (Fig. 5(d) [48]) and a particle-free air protection box (Fig. 5(e) [49]) were designed to reduce PM contamination and ozone generation on the high-voltage tip electrodes [48,49].

3.3. Electrostatically responsive fiber

As indicated in Eq. (6), F_E on the PM (acting as the mass transfer force) is influenced by the relative dielectric constant of the fibers (ε_f) when the PM is close to the fibers. Experiments demonstrated a positive correlation between ε_f and the filtration efficiency enhanced by PM charging and fiber polarization [50]. Besides, the

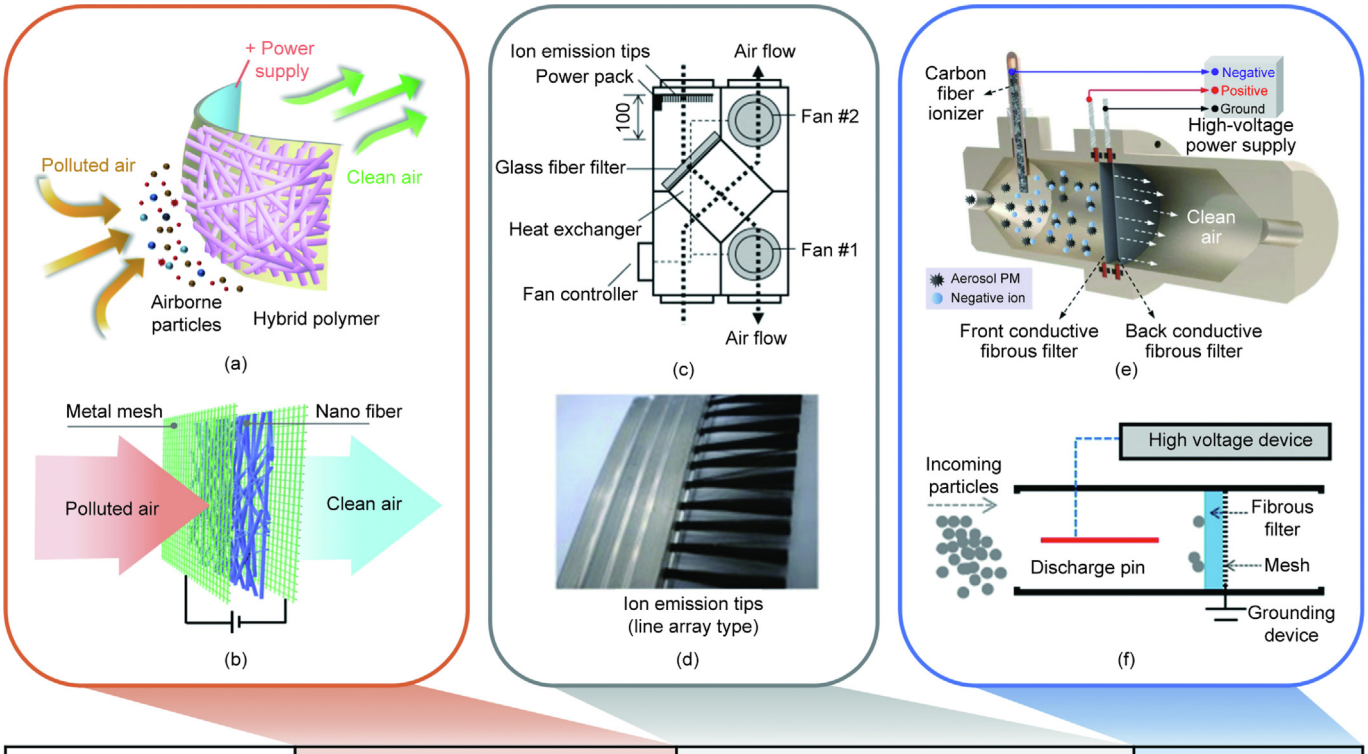

Charge on PM	0	q_p	q_p
Electric field around fibers	E	0	E
Type of electrostatic force	Dielectrophoretic force	Image force	Coulomb force
Equation of electrostatic force	$F_D = \frac{\pi\varepsilon_0 d_p^3}{4}\left(\frac{\varepsilon_p - 1}{\varepsilon_p + 2}\right)\nabla\lvert E\rvert^2$	$F_I = \frac{q_p^2}{4\pi\varepsilon_0}\left(\frac{\varepsilon_f - 1}{\varepsilon_f + 1}\right)\frac{1}{(2r - d_f)^2}$	$F_E = q_p E$

Fig. 3. Electrostatic filtration technologies categorized by the electrostatic force types. (a) An air filter enhanced by tribo-charge [34]. (b) An air filter charged by induction [35]. (c) An ionizer-assisted air filter in a heating, ventilating, and air conditioning (HVAC) system, and (d) a photo of the ionizer [36]. (e) Capturing charged PM with conductive filters [37]. (f) A pin-to-filter-to-ground charging device [38]. Reproduced from Refs. [34–38] with permission. The definitions of all the abbreviations in the figure could be found in the cited references [34–38].

EAA filtration is influenced by factors such as fiber distribution and pore distribution. Notably, even when the pressure drops of filters are comparable (11.6 to 16.9 Pa at 1.1 $m \cdot s^{-1}$), the electrostatically assisted filtration efficiency for $PM_{0.3-0.5}$ can vary significantly from 50.6% to 95.4% [45]. Therefore, the design of the fibrous material is essential to the system-level performance of the EAA filtration devices.

We proposed a concept of "electrostatically responsive filters" involving coating a small quantity of heterogeneous material with a high relative dielectric constant onto the fibers with low air resistance (Fig. 6(a)) [41]. The fibrous material can maintain a large physical porosity after coating to sustain its low wind-pressure drop. High-dielectric-constant caking results in much more induced charges on their surface in a polarizing electric field (Fig. 6(b) [41]). This phenomenon facilitates the migration and capture of charged PM, enhancing the PM filtration efficiency. In this way, inexpensive coarse filters can be transformed into highly efficient electrostatically responsive filters with low wind-pressure drop, making the best use of the material.

The preparation methods for electrostatically responsive filters can be categorized into physical and chemical. In physical methods, a high-dielectric-constant material is coated onto the fiber through physical adhesion (Figs. 6(c) and (e) [51]). Tian et al. [41] employed a rapid and extensive roll-to-roll gel squeezing technique to incorporate manganese dioxide, activated carbon (AC), zinc oxide, copper oxide, and barium titanate onto polyurethane (PU) foams. The MnO_2-coated polyurethane foams demonstrated 82.5% removal efficiency of undesired ozone produced during PM charging [51]. The physical method usually exhibits a higher loading capacity, shorter preparation time, and lower cost for large-scale production. However, the coatings can be easily released due to the absence of chemical bonding between the high-dielectric-constant material and the fiber substrate. Consequently, the physical method may not be applicable in specific scenarios that demand exceptionally high filtration efficiency, such as cleanrooms.

In the chemical method, a high-dielectric-constant material grows on the fiber, forming a stronger chemical bond. Tian et al.

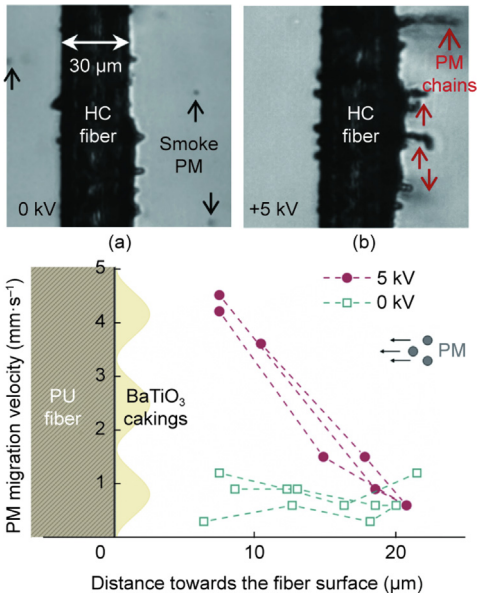

Fig. 4. The photographs of PM migrating towards the heterocaking (HC) fibers when (a) 0 and (b) 5 kV were applied to the device. (c) The PM migrating velocity to the HC fiber [41]. PU: polyurethane. Reproduced from Ref. [41] with permission.

[46] grow thin polydopamine (PDA) coatings on the polyethylene terephthalate (PET) coarse filter through *in situ* dopamine polymerization, achieving a high filtration efficiency of 99.48% for $PM_{0.3–0.5}$ and a low wind-pressure drop of 9.5 Pa at 0.4 $m·s^{-1}$ filtration velocity. Dong et al. further doped the PDA-coated PET with MOF crystals via suction filtration [52]. Gao et al. [53] doped the PDA-coated PET with manganese oxide (MnO_x) via dip-coating of potassium hypermanganate precursors (Figs. 6(d) and (f) [53]), demonstrating a 96.8% removal efficiency for 100 ppb level ozone. While chemical approaches provide solutions for coating release, they tend to be expensive and time-consuming, thus posing challenges for achieving large-scale manufacture.

3.4. Improved PM filtration performance

Compared to commercial filter materials with similar filtration efficiency for $PM_{0.3–0.5}$, EAA filters illustrated a significant reduction in air resistance, ranging from 1 to 3 orders of magnitude (Fig. 7(a) [41,45–48,50,51,53–57]). However, it is inappropriate to compare EAA filters with conventional filters in quality factor (QF), which incorporates the ratio between the benefit (filtration efficiency) and the payout (wind-pressure drop) for evaluating the overall performance of filtration materials (Eq. (7)). As EAA filtration consumes additional energy for creating electric fields apart from the fan energy consumption, Tian et al. proposed a comprehensive quality factor (CQF) by assuming that the extra energy consumption for filtration efficiency improvement is equivalent to an extra equivalent pressure drop (Eq. (8)) [54]:

$$QF = \frac{-\ln\left(1-\eta_f\right)}{\Delta p} \tag{7}$$

$$CQF = \frac{-\ln\left(1-\eta_f\right)}{\Delta p + \frac{\eta_{fan} P_E}{v_{air}}} \tag{8}$$

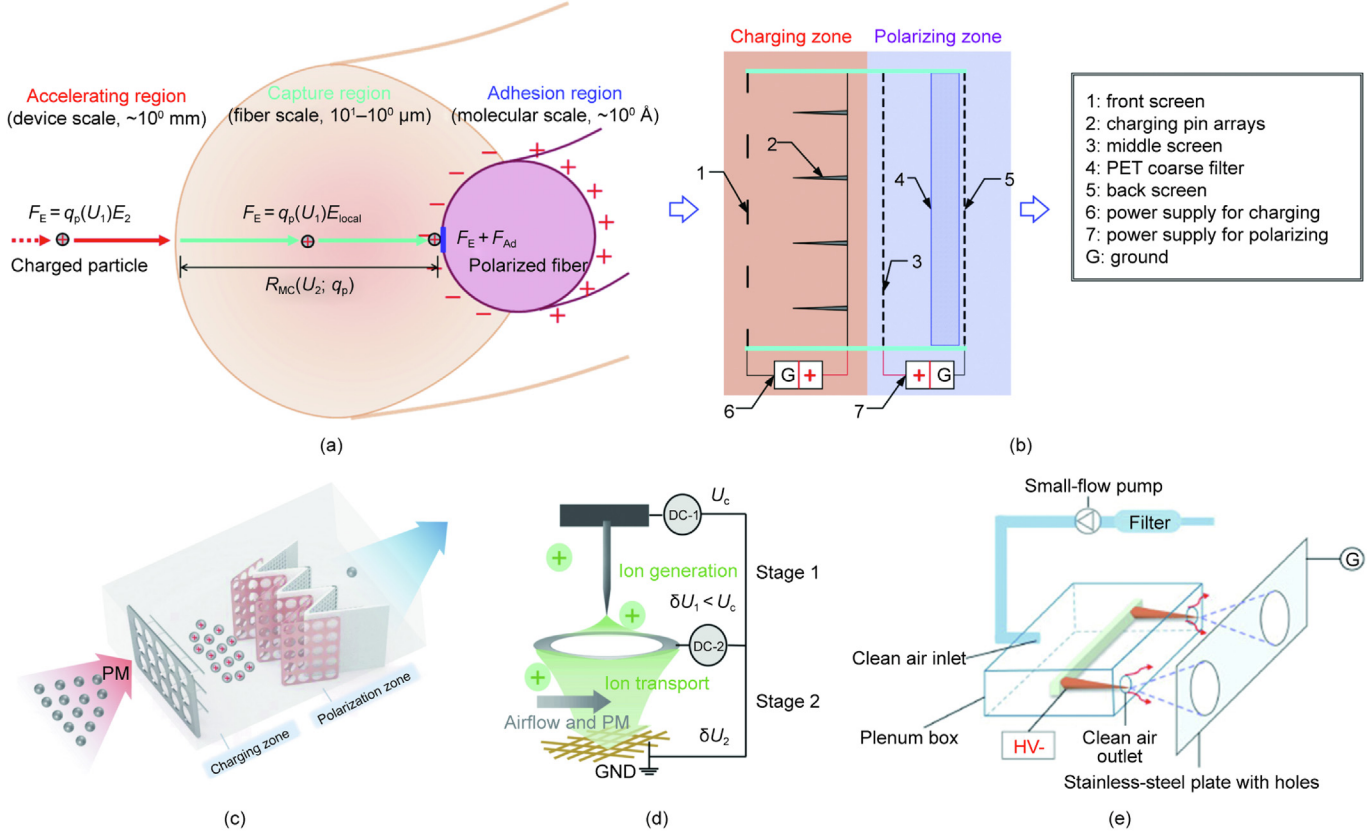

Fig. 5. (a) The migration of a charged PM towards a dielectric fiber in an electric field [46]. The schematics for (b) the two-stage EAA filter [45] and (c) the EAA filter with a W-shaped polarization zone [47]. (d) The two-stage cascaded corona discharger [48] and (e) the particle-free air protection enclosure for the discharger [49]. U_c: voltage for particle charging; DC: direct current (power supply); GND: ground; HV: high-voltage (power supply). Reproduced from Refs. [45–49] with permission. The definitions of all the abbreviations in the figure could be found in the cited references [45–49].

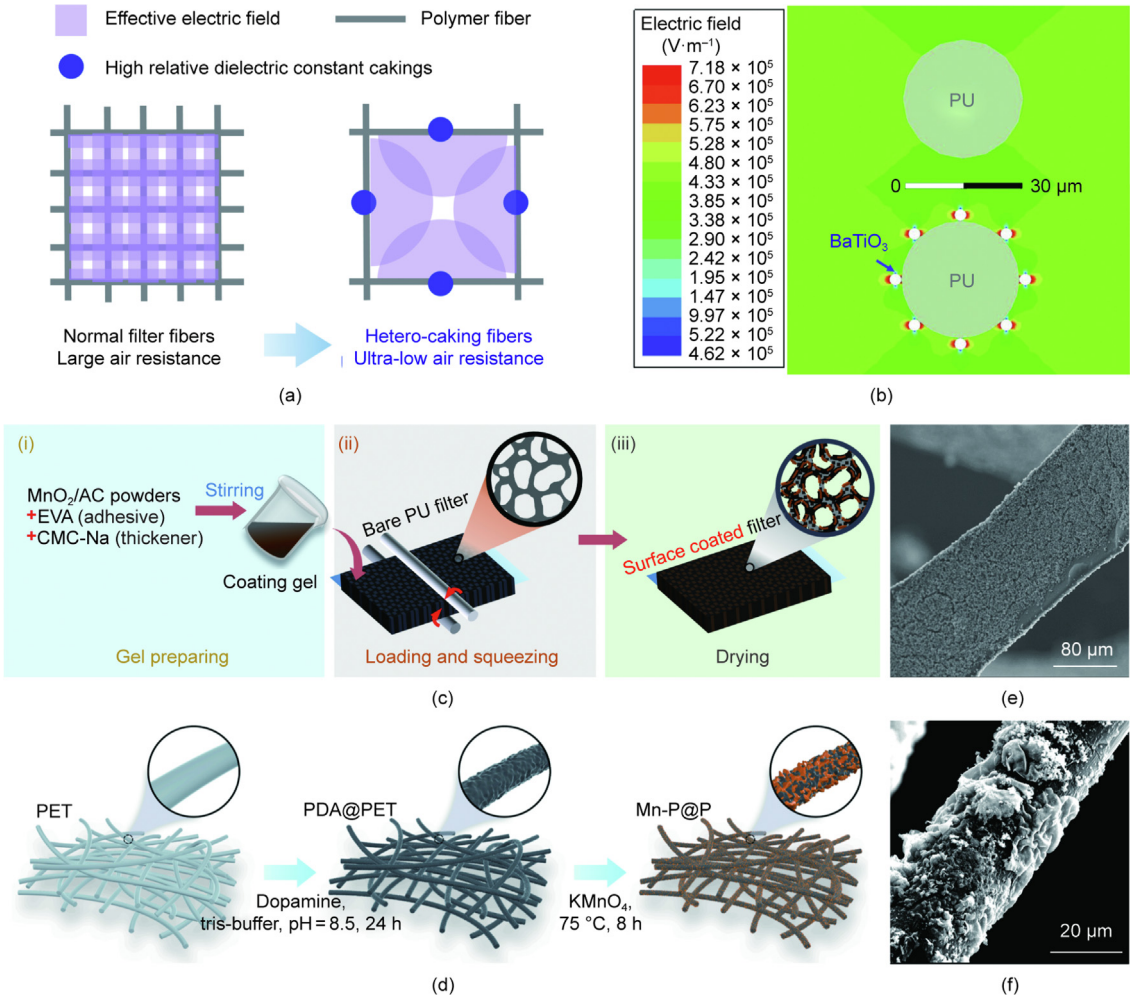

Fig. 6. (a) Schematic of electrostatically responsive filters compared with normal filter fibers. (b) The simulated electric field around the polarized bare PU fiber (up) and $BaTiO_3$-coated PU fiber (down) [41]. Schematics of (c) the roll-to-roll gel squeezing preparation method to coat filters [51] and (d) the chemical preparation method to grow coatings on fibers [53]. The scanning electron microscope (SEM) images of (e) the MnO_2-coated PU fiber [51] and (f) the MnO_x on grow thin polydopamine (PDA)-coated PET fiber [53]. Reproduced from Refs. [41,51,53] with permission.

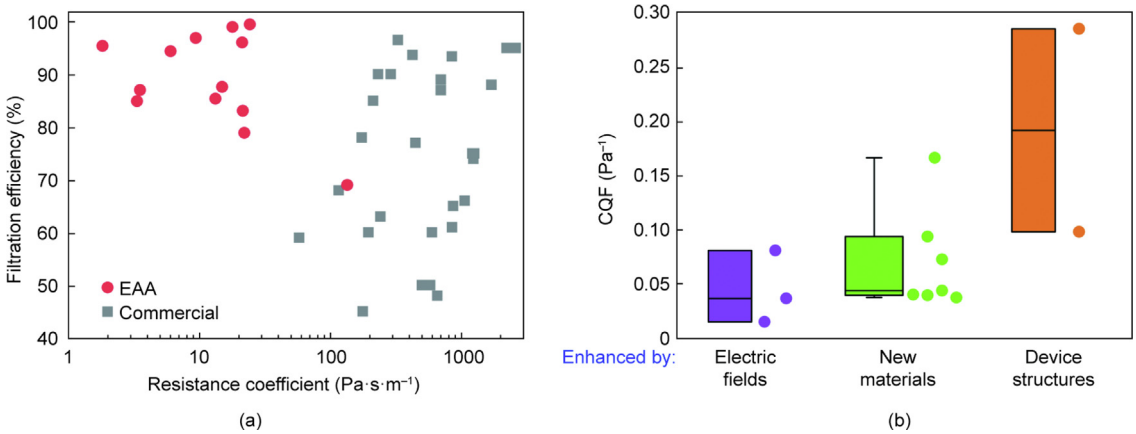

Fig. 7. (a) Performance comparison of EAA filters from Refs. [41,45–48,50,51,53–57] and commercial filters from Ref. [31]. The resistance coefficient is obtained by dividing the Δp by the v_{air}. (b) CQF of EAA filtration studies in which performance is enhanced mainly by enhancing the electric fields, developing new materials, and designing the device structures.

where η_{fan} is the estimated efficiency of the fan in an HVAC system, 0.71; P_E ($W \cdot m^{-2}$) refers to the energy consumption for creating electric fields in an air filtration device.

The research on EAA filtration can be categorized into three types for different method to improve the performance: external mass transfer enhancement, materials enhancement, and structure enhancement. Substantial improvements in CQF existed with the advancement of electrostatically responsive new materials and device structural designs (Fig. 7(b)). A study from Germany rated the EAA filter research as "very good" in a relevant review for

indoor environments [58]. Due to the limited research on device structures, further investigations are necessary to enhance the overall performance and our understanding of EAA filtration techniques.

Several existing surface modification techniques can be applied to the future development of electrostatically responsive fibers, such as electrospinning [59] and self-polarized assembly technique [60]. Nevertheless, some may not be suitable or require improvement when utilizing coarse fibrous materials as substrates, primarily due to their huge pore size. Examples of such techniques include scrape, spin, and slot coating. Moreover, considering the low cost and limited resistance to high temperatures, air filter substrates are not appropriate for expensive surface modification techniques that involve high-temperature procedures, such as atomic layer deposition and chemical vapor deposition. Therefore, further exploration is required to build a low-cost and scalable surface modification method for electrostatically responsive fibrous materials. Moreover, assessing the porosity, pore size distribution, surface morphology, and surface voltage potential is challenging with conventional methods. Therefore, it is essential to clearly understand the relationship between parameters and the performance of electrostatically responsive filters through thorough characterization and principled investigations.

4. Improving indoor gaseous pollutant removal by multiscale mass transfer enhancement

Extensive research has been carried out on gas adsorption, including gas separation, CO_2 capture, and removal of indoor gaseous pollutants [61–63]. Catalysis can complement adsorption as an effective method for enhancing the sustainability of gas purification or separation processes [64]. However, conventional adsorptive and catalytic materials produced via granulation frequently encounter issues related to elevated air resistance, resulting in increased energy consumption. Monoliths, characterized as multilayered net-like structures with interconnecting channels, have been increasingly utilized as adsorption components to address these limitations [65]. The hierarchical porous structures of monoliths and the consequent large gas-solid interfacial contacting areas facilitate improved mass transfer kinetics and significantly reduce pressure drop compared with granular adsorption/catalytic components [66]. This section focuses on the impact of such monolithic structures on the mass transfer process in adsorption and catalysis, thereby improving the removal of gaseous pollutants. The relevant materials and manufacturing process are summarized.

4.1. Mass transfer in gas adsorption and catalysis

Insufficient mass transfer may reduce the concentration gradient of target gas or reactants on the gas-solid interfaces of the materials [67], thus slowing down the adsorption flux and the reaction rates. Enhancing mass transfer kinetics is more economically viable through modifications to the geometric structures and internal porous architecture of adsorption components rather than concentrating on developing high-performance materials with high specific surface area or particular functional groups [68]. In adsorption and catalytic beds, materials typically form into beads with 10^3–10^4 μm diameters. The specified size maintains an adequate distance between particles, preventing excessive air resistance [69].

Fig. 8 [70] (up) illustrates that the millimeter-sized beads had a long diffusion path for gas molecules, resulting in diffusion resistance being the primary limitation in the overall adsorption mass transfer process. Generally, a smaller pore size is beneficial for producing a larger specific surface area but is not conducive to mass

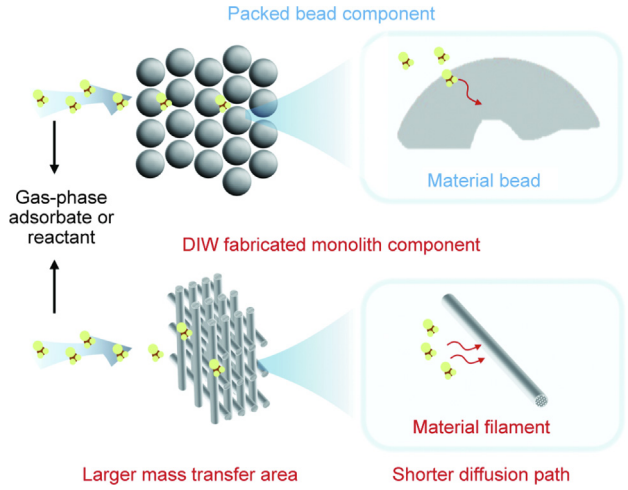

Fig. 8. Mass transfer process of gas molecules inside the packed bed and the monolith. Reproduced from Ref. [70] with permission.

transfer. An ideal porous adsorbent should have a uniform structure with micropores (< 2 nm) and hierarchical pores (mesopores, 2 nm < pore size <50 nm; macropores, pore size > 50 nm) [71]. This design maximizes surface area for the distribution of active sites, reduces mass transfer resistance, and enhances access to micropores. However, the pores inside the adsorbent are mainly within the range of 10^{-1}–10^{0} nm [72]. The sizes are less than the average free path of most indoor air pollutants, such as formaldehyde and toluene [73], resulting in slow diffusion rates. The considerable mass transfer resistance inside the material leads to the concentration accumulation at the gas-material interfaces, reducing the gas concentration gradient and, consequently, the mass transfer flux.

Novel adsorbent structures are significant for improving the mass transfer kinetics. For example, the monolith structure with a millimeter–micron–nanometer morphology, a novel honeycomb-like structure consisting of filaments with gaps in 10^2 μm (Fig. 8, down), can offer several advantages for enhancing adsorption mass transfer. ①The monoliths reduce the gas diffusion path at the macro level compared to the densely packed adsorbent, thereby decreasing gas molecule transport durations. This reduction in inner diffusion resistance mitigates the decline in mass transfer flux. Besides, the honeycomb structures provide sufficient gas-solid interfacial contact, expanding the mass transfer area and enhancing the overall adsorption/catalysis performances [74,75]. ②At the micro and nano scales, optimizing the pore distribution within the porous material, such as increasing the average pore size and providing diffusion channels ranging from hundreds of nanometers to several microns, can accelerate the rapid diffusion and migration of adsorbate molecules inside the porous material. However, achieving this ideal multi-scale structural design requires careful consideration of material selection, preparation procedures, and component structure, which necessitates further investigation. Besides, manufacturing these specifically designed porous monoliths using conventional techniques is challenging due to limitations in fabrication resolution.

Besides, the external field force also promotes gas mass transfer. For instance, non-thermal plasma and the associated ionic wind effect can potentially enhance mass transfer in gas adsorption and catalysis [76,77]. The electric field generated by the non-thermal plasma creates an ionic wind that promotes convective mass transfer, leading to more efficient delivery of pollutants to the catalyst/adsorbent surface [78]. This enhanced transport overcomes diffusion limitations, particularly in scenarios with low flow rates or stagnant boundary layers.

4.2. Preparation of adsorbents/catalysts via direct ink writing (DIW)

Traditionally, monolithic adsorbents and catalysts are manufactured using hydraulic extrusion technology [79]. However, the geometry of the extrusion heavily depends on the pre-fabricated die, requiring additional procedure, equipment, and time. This limitation constrains the geometric flexibility of purification equipment and hinders the material's versatility. DIW, a three-dimensional (3D) printing technique, has been widely utilized for its diverse suitable materials, cost-effectiveness, and fast production [80].

In the DIW process, it is essential to choose appropriate adsorbents or catalysts to formulate a printable suspension, which is also known as printing ink. The rheological properties, including dispersion, viscosity, and viscoelasticity, should be meticulously determined to guarantee a smooth printing process [81]. Adding appropriate dispersants, binders, and plasticizers effectively enhances the rheological property and the consequent printing product [82]. For DIW-fabricated monoliths, the gas molecule diffusion inside the adsorbent becomes challenging due to the high internal diffusion mass transfer resistance. The reason is that the intrinsic pore size of the porous adsorbent is concentrated at 10^{-1}–10^{0} nm, which is shorter than the mean free path of the gas molecules diffused in it. Consequently, gas molecules are continually captured and desorbed by the pore wall during the diffusion, leading to a winding diffusion path and presenting a high resistance in diffusion (known as Knudsen diffusion) [83]. To enhance the diffusion mass transfer, building more pores within the diameter range of 10^{-1}–10^{0} μm in the material is essential.

At present, the primary methods to achieve pore regulation in printed adsorbent materials are the gas volatilization method (Fig. 9(a)) and the sacrificial template method (Fig. 9(b)). The gas volatilization method is realized by adding a material to the ink that can decompose and generate gas. After printing, the gas can be generated by controlling the temperature of the printing platform [22] so that the pores would form inside the adsorbent. In the sacrificing template method, a template material is premixed into the ink and removed after printing to form pores. As shown in Fig. 9(c), Chen et al. [22] added ammonium carbonate to the adsorbent ink and heated it to generate NH_3 and CO_2 after printing. The generated gas could form micron-sized pores inside the printed adsorbent (Figs. 9(d)–(e) [22]), and the inward gas diffusion rate of the adsorption film could accelerate. In another approach, Huang et al. [84] utilized micro-nano-sized polymethyl methacrylate (PMMA) beads as the sacrificial template. The beads were first suspended in the polymethylsiloxane/isopropanol solutions to formulate ink and then removed in a high-temperature inert atmosphere (99.99% N_2) following the printing (Fig. 9(f)). As shown in Figs. 9(g)–(h) [84], the porosity and pore size of the material could be tailored by changing the size and amount of the PMMA beads [27,84]. By combining the gas volatilization and sacrifice template methods, DIW can construct adsorption components with multi-scale morphology from millimeter to micron to nanometer.

Additional post-processing methods, including surface loading and grafting, are extensively used to enhance gas–solid interactions via specialized physical and chemical interactions [85]. For example, Lawson et al. printed and infused the MOF monolith with

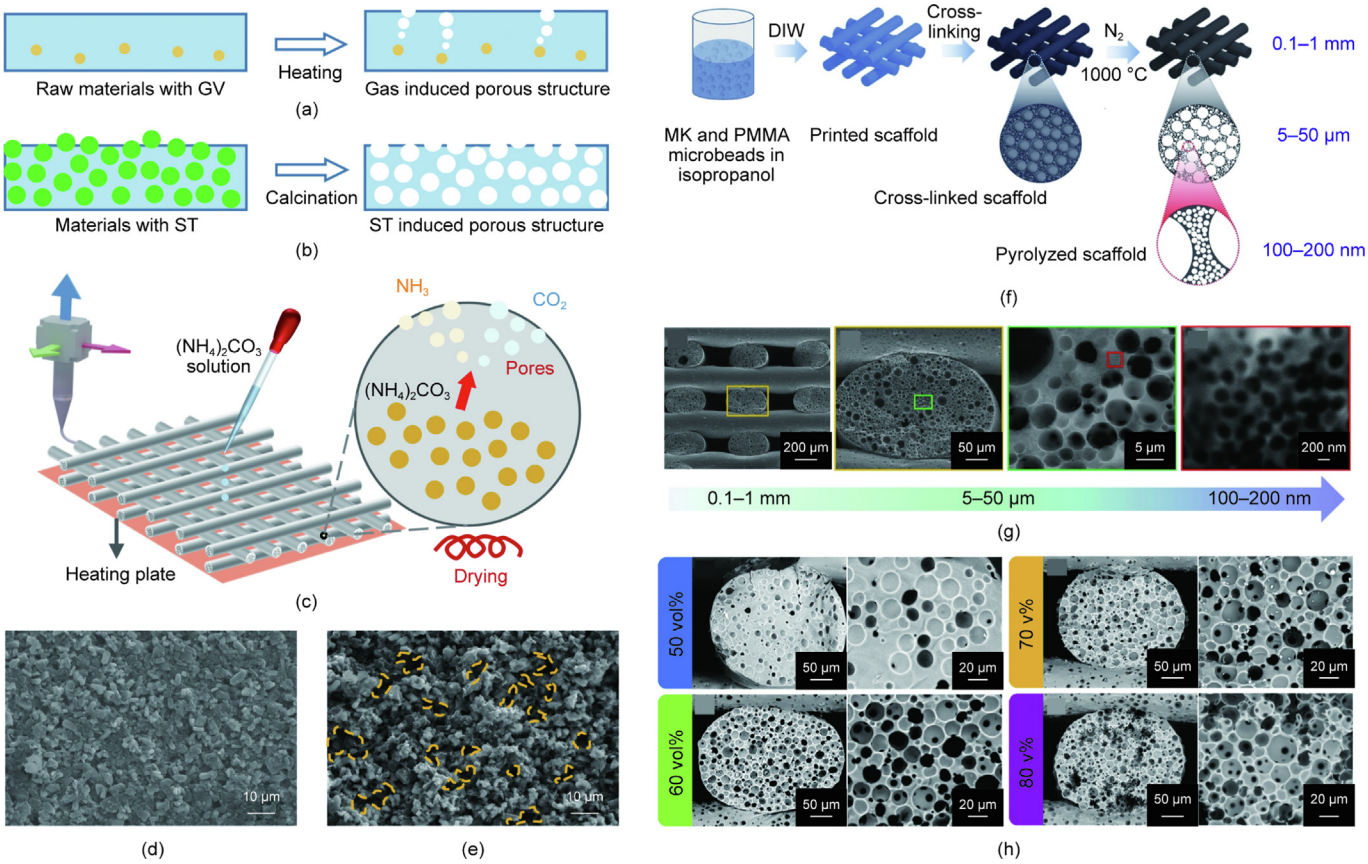

Fig. 9. The schematics of (a) the gas volatilization and (b) the sacrificial template regulation methods. (c) The ammonium carbonate decomposition induced pores inside the adsorbent. The SEM images of the pores inside the adsorbent (d) before and (e) after the ammonium carbonate processing [22]. (f) The pore size regulation by PMMA beads as a sacrificial template. (g) The SEM images of the tailorable pore size distribution and (h) porosity tailored by adjusting the size and amount of the sacrificial template [84]. Reproduced from Refs. [22,84] with permission.

amine-dense tetraethylenepentamine (TEPA) or polyethyleneimine (PEI), achieving high CO_2 adsorption capacities of 1.8 and 2.8 mmol·g^{-1}, respectively [86]. Medina et al. [87] developed a hyper-crosslinked adsorption monolith by adhering hyper-porous carbon powder to the printed polymer monolith. Pellejero et al. used atomic layer deposition to apply ZnO nanosheets on the printed honeycomb filters, and zeolitic imidazolate framework-8 (ZIF-8) can be obtained via *in situ* hydrothermal synthesis on ZnO, allowing for efficient VOC removal [88].

4.3. Improving adsorption performance by structural enhancement

Recent progress in indoor gas adsorption materials includes activated carbon, ceramic adsorbents, MOFs, and polymer adsorbents [89]. These materials are utilized in different structures, including packed adsorption beds, fiber adsorption components, and monolithic adsorption components. The packed adsorption bed is the most widely used component due to its simple structure and convenient manufacturing [90]. It can achieve a lifetime of more than 60 h with high-performance materials loaded [91]. However, densely packed adsorption beds face relatively high resistance, leading to poor mass transfer kinetics and low utilization rates of adsorbed materials [92], resulting in rapid decay in most cases [93–95]. The lifespan of fiber adsorbers is generally shorter because the thickness of typical fibers is limited [96], and excessively thick fibers introduce high wind resistance [97], making them more challenging for application. In many studies, the surface velocity is maintained very low, typically ranging from 10^{-3} to 10^{-2} m·s^{-1}, resulting in an initial pass efficiency of 100% [74,90,94,95,98]. However, the breakthrough performances declined rapidly, many falling within 10 h and some even within 1 h [74,93,94,98].

To overcome this, Chen et al. [99] developed a laminated adsorption component by assembling temperature-controllable films coated with adsorbent (adsorption films) in parallel (Fig. 10(a) [99]). This structure resembles a monolith construction, where gas flows through channels, and the monolith adsorbs the target gas. Once the adsorbent saturates, adsorption films can undergo *in-situ* electro-thermal regeneration. Compared to the traditional regeneration method, which preheats the airflow first and subsequently heats the material, *in-situ* thermal regeneration has been proven more energy-efficient owing to reduced heat dissipation and heightened regeneration efficiency [99]. The film-structured adsorption component can achieve 82% and 81% single-pass removal efficiency for formaldehyde and toluene at 0.8 m·s^{-1} face air velocity [22].

The adsorption capacity of gaseous pollutants is influenced by both the equilibrium adsorption capacity and the dynamic adsorption capacity. The equilibrium adsorption capacity is primarily determined by the specific surface area (SSA) of the adsorbent, which decreases as pore size increases. Micropores (pore size < 2 nm) provide a significantly larger SSA compared to mesopores (2 nm < pore size < 50 nm) and macropores (pore size > 50 nm). However, the small size of micropores can limit the diffusion rate of gaseous pollutants, such as formaldehyde and toluene, due to their average free path being larger than the pore diameter [73]. In contrast, the dynamic adsorption capacity, which reflects the adsorption amount [101] and the capturing rate, is more critical in real-world applications. To optimize dynamic adsorption capacity, an ideal adsorbent should possess a hierarchical pore structure that balances high SSA (for equilibrium adsorption) and efficient mass transfer (for dynamic adsorption) [22,102]. Increasing the mesoporous ratio under similar porosity conditions can enhance diffusion rates [103], but an excessively high mesoporous ratio may reduce the SSA and compromise the equilibrium adsorption capacity. Therefore, achieving an optimal pore size distribution is essential to maximize the dynamic adsorption capacity, requiring a careful balance between diffusion efficiency and equilibrium adsorption performance.

Chen et al. employed laser etching to create submillimeter-scale vertical penetration channel structures on the adsorption film (Figs. 10(b)–(e)) [100]. Formaldehyde and xylene were chosen as

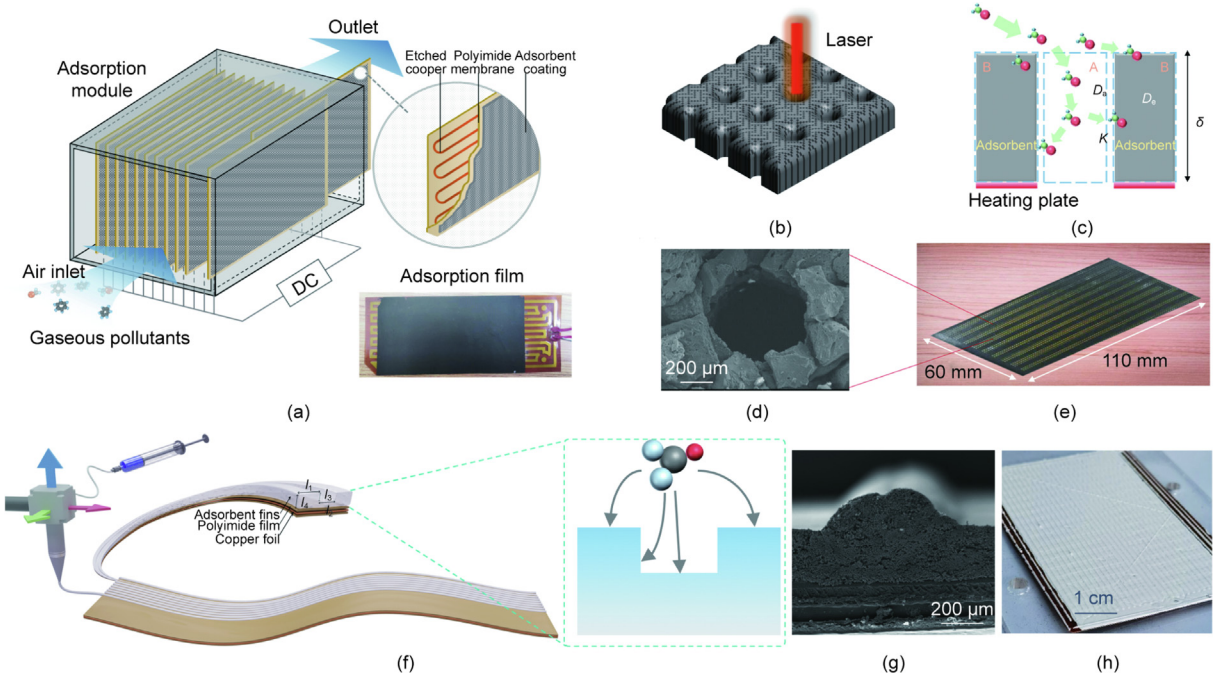

Fig. 10. (a) The schematic of the laminated adsorption component built by adsorption films [99]. (b) A submillimeter-scale vertical penetration channel structure created on the adsorption film using laser drilling. (c) The mass transfer process of the adsorption film with submillimeter-scale vertical channels. (d) SEM image of the submillimeter-scale vertical penetration channel structure and (e) a physical photo of the channel-structured adsorption film [100]. (f) DIW molded sub-milli ribbed adsorption films. (g) The SEM image and (h) physical photo of the rib structure [20]. Reproduced from Refs. [20,99,100] with permission.

the target adsorbates. The two pollutants were limited in the China National Standard GB/T 18883 and are most widely studied for indoor VOC adsorptive removal [104,105]. Additionally, the adsorption properties of xylene can reflect the purification capabilities of adsorption materials for benzene, toluene, and other aromatic compounds [100]. Compared to adsorbents without channel structures, the adsorption capabilities for formaldehyde and xylene were enhanced by 100% and 80%, respectively. Physical adsorption was demonstrated by X-ray photoelectron spectroscopy and X-ray diffraction spectrum, showing no new functional groups or chemical bonds forming after formaldehyde and toluene adsorption [22]. Therefore, the adsorption films can be extended to other gaseous pollutants, making it a widely available method for air purification. Besides, the adsorption film can be modularized into a laminated structure and scaled to a normalized adsorption module. The efficiency of the adsorption module remains consistent regardless of size, while the airflow volume and pollutant removal rate increase in direct proportion to the windward area [102].

Furthermore, a sub-milli ribbed structure was constructed on the adsorption films using the DIW method (Figs. 10(f)–(h)) [20]. The ribbed structure effectively increases the gas–solid contact area by 58% and accelerates mass transfer by enhancing the airflow turbulence. Experimental results indicate a 37% increase in the one-pass efficiency of formaldehyde, leading to a remarkable enhancement in dynamic adsorption capacity by 152%. Through interfacial structural modification and internal pore regulation, the sub-milli-net hierarchical-porous adsorption plate (SHARP) can achieve outstanding mass transfer kinetics in conjunction with the inherent nanopores of the material. The gradient porous structures in SHARP are promising not only in the field of indoor air purifying but also in broader energy and environmental studies due to their adequate heat and mass transfer dynamics [106]. Similarly, Tammaro et al. combined 3D printing with foaming technology, which made a 20% increase in surface area from 255 to 314 m^{-1}, showing a 96.0% removal efficiency for 500 ppm SO_2 at 0.13 $m^3 \cdot h^{-1}$ flow rate [107]. Besides, the integration of internal cooling can further improve 28.42% benzene removal performance, primarily due to the reduction in liquid desiccant solution temperature and the corresponding decrease in Henry's constant, which enhances the driving force for benzene transfer from air to the desiccant solution [108]. Humidity regulation is also essential for improving mass transfer efficiency by reducing the competitive adsorption of water molecules on the catalyst surface, which otherwise obstructs the adsorption and activation of volatile organic compounds such as toluene [109].

5. Conclusions and perspectives

Traditionally, air pollution purification has focused on the qualities of the materials themselves, often neglecting the importance of mass transfer, which ultimately results in high air resistance. This study summarized the novel approach that shifts from passive material usage to active control of mass transfer, setting out to better understand bridging the gap between high-performance materials and high-performance technologies. The main viewpoints can be summarized as follows:

(1) Significance of mass transfer enhancement. This study highlights that optimizing mass transfer can significantly improve air purification technologies' efficiency and energy performance. For PM removal, we suggest using electrostatic assistance in filtration, which can enhance the migration velocity of PM towards the fibers, resulting in 1–3 orders of magnitude higher CQF compared to commercial filters. We suggest constructing hierarchical structures for gas-phase pollutant removal, which can increase the gas-solid contact area by 58%, leading to a 37% improvement in single-pass removal efficiency and a 152% enhancement in dynamic adsorption capacity.

(2) Approaches to mass transfer enhancement. This study highlights optimizing mass transfer through multiscale (milli–micro–nano) and multifield (mass–flow–force) approaches. The physical fields may include electric, magnetic, thermal, microwave, and ultrasonic fields. These physical fields can improve mass transfer efficiency by influencing the adsorption kinetics, reducing the diffusion boundary layer thickness, and modifying the interactions between adsorbents and adsorbates.

(3) Other influencing factors in real-world applications. Organic pollutants such as VOCs can affect the adsorption performance by occupying the pores of purification materials, thereby reducing the effective surface area available for adsorption. Additionally, these pollutants can alter the dielectric properties of materials, impacting the electrostatic field's enhancement of mass transfer. Besides, limited indoor space often necessitates the tight compression of purification components, increasing air resistance but enhancing contact between pollutants and materials. Balancing space constraints, resistance, and mass transfer performance is a critical challenge. Furthermore, the ventilation rate (face velocity) significantly influences pollutant-material contact time, thus strengthening or weakening mass transfer. Optimal air flow rates should be determined in different ventilation circumstances to ensure a sufficient clean air supply and efficient mass transfer.

(4) Future research and application guidelines. Future research should focus on developing new interaction mechanisms, innovative fabrication methods, and optimized ventilation strategies to further advance the field. For future applications, substantial implementation expenses, the need for specialized apparatus, and a lack of skilled staff may impede adoption. The long-term performance and stability of EAA filtration and SHARP systems should be further evaluated. Research and development should prioritize cost-effective solutions to address these challenges, and collaborations between industry and academia should be enhanced. The insights and methodologies presented in this study have the potential to revolutionize indoor air purification and contribute to broader applications in various sectors, including chemical, pharmaceutical, and environmental industries.

CRediT authorship contribution statement

Enze Tian: Writing – review & editing, Visualization, Conceptualization, Writing – original draft, Funding acquisition. **Qiwei Chen:** Writing – original draft, Visualization. **Yilun Gao:** Visualization, Data curation. **Zhuo Chen:** Writing – review & editing. **Yan Wang:** Writing – review & editing. **Jinhan Mo:** Writing – original draft, Funding acquisition, Writing – review & editing, Supervision, Conceptualization.

Declaration of competing interest

The authors declare that they have no known competing financial interests or personal relationships that could have appeared to influence the work reported in this paper.

The author is an Editorial Board Member for *Scientific Reports*, an Associate Editor for National Science Open, a Subject Editor for *Building Simulation*, a Guest Editor for *Building and Environment*, and was not involved in the editorial review or the decision to publish this article.

Symbols

A^*	Dimensionless characteristic surface area for mass transfer
CADR	Clean air delivery rate, $m^3 \cdot s^{-1}$
CQF	Comprehensive quality factor, Pa^{-1}
C_∞	Pollutant concentration in the inflow, $mg \cdot m^{-3}$
$C_{interface}$	Pollutant concentration on the interface of airborne pollutants to the materials, $mg \cdot m^{-3}$
d_f	Fiber diameter, m
d_p	Particle diameter, m
E	Electric field intensity, $V \cdot m^{-1}$
E_∞	External electric field intensity, $V \cdot m^{-1}$
E_{local}	Local electric field intensity, $V \cdot m^{-1}$
F_{Ad}	Adhesion force, N
F_D	Dielectrophoretic force, N
F_E	Coulomb force, N
F_I	Image force, N
G	Airflow rate, $m^3 \cdot s^{-1}$
h_m	Convective mass transfer coefficient, $m \cdot s^{-1}$
L	Thickness, m
NTU_m	Number of mass transfer units
P_E	Energy consumption for creating electric fields, $W \cdot m^{-2}$
q_p	Charges on the PM, C
QF	Quality factor, Pa^{-1}
r	Distance, m
R_{MC}	Monopole capture distance, m
St_m	Stanton Number for mass transfer
U_1	Applied voltage for particle charging, V
U_2	Applied voltage for fiber polarizing, V
α	Fiber volume percentage in the filter
Δp	Pressure drop, Pa
ε_0	Vacuum permittivity, 8.85419×10^{-12} $F \cdot m^{-1}$
ε_f	Relative dielectric constant of the fiber
ε_p	Relative dielectric constant of the particle
ϕ	Mass transfer flux per unit area, $mg \cdot m^{-2} \cdot s^{-1}$
η	Dimensionless coefficient related to material properties
η_f	Filtration efficiency
η_{fan}	Fan efficiency
η_s	Filtration efficiency of a single-cylinder fiber
μ	Air viscosity, Pa·s
v_{air}	Face air velocity over the filter, $m \cdot s^{-1}$

Acknowledgments

This work was financially supported by the National Natural Science Foundation of China (52325801 and 52408122), Shenzhen Natural Science Foundation (JCYJ20240813143502004), and the Guangdong Basic and Applied Basic Research Foundation (2022A1515110897).

References

[1] Chen Z, Xia F, Fan Y, Jiang Y, Xu Y, Mo J. Partitioning mechanisms and film formations of DEHP on realistic indoor airborne particles and road dust. Build Environ 2024;252:111273.
[2] Sikka MP, Mondal M. A critical review on cleanroom filtration. Res J Text Appar 2022;26(4):452–67.
[3] Lu D, Luo Q, Chen R, Zhuansun Y, Jiang J, Wang W, et al. Chemical multi-fingerprinting of exogenous ultrafine particles in human serum and pleural effusion. Nat Commun 2020;11(1):2567.
[4] Xue Y, Wang L, Zhang Y, Zhao Y, Liu Y. Air pollution: a culprit of lung cancer. J Hazard Mater 2022;434:128937.
[5] Gao X, Coull B, Lin X, Vokonas P, Spiro A, Hou L, et al. Short-term air pollution, cognitive performance and nonsteroidal anti-inflammatory drug use in the Veterans Affairs Normative Aging Study. Nat Aging 2021;1(5):430–7.
[6] Al-Kindi SG, Brook RD, Biswal S, Rajagopalan S. Environmental determinants of cardiovascular disease: lessons learned from air pollution. Nat Rev Cardiol 2020;17(10):656–72.
[7] Lewis AC, Jenkins D, Whitty CJM. Indoor air pollution: five ways to fight the hidden harms. Nature 2023;614:220–3.
[8] Hoefflinger B. ITRS: the international technology roadmap for semiconductors. In: Hoefflinger B, editor. Chips 2020: a guide to the future of nanoelectronics. Heidelberg: Springer; 2012. p. 161–74.
[9] Wang F, Permana I, Lee K, Rakshit D, Rosulindo PP. Improvement of airflow distribution and contamination control for a biotech cleanroom. Atmosphere 2022;13(2):335.
[10] Lindsley WG, Derk RC, Coyle JP, Martin SB, Mead KR, Blachere FM, et al. Efficacy of portable air cleaners and masking for reducing indoor exposure to simulated exhaled SARS-CoV-2 aerosols—United States, 2021. MMWR Morb Mortal Wkly Rep 2021;70:972–6.
[11] Blocken B, van Druenen T, Ricci A, Kang L, van Hooff T, Qin P, et al. Ventilation and air cleaning to limit aerosol particle concentrations in a gym during the COVID-19 pandemic. Build Environ 2021;193:107659.
[12] Yin J, Liu X, Guan B, Zhang T. Performance and improvement of cleanroom environment control system related to cold–heat offset in clean semiconductor fabs. Energy Build 2020;224:110294.
[13] Zhuang C, Shan K, Wang S. Coordinated demand-controlled ventilation strategy for energy-efficient operation in multi-zone cleanroom air-conditioning systems. Build Environ 2021;191:107588.
[14] Burgard M, Weiss D, Kreger K, Schmalz H, Agarwal S, Schmidt H-W, et al. Mesostructured nonwovens with penguin downy feather-like morphology—top-down combined with bottom-up. Adv Funct Mater 2019;29(34):1903166.
[15] Niu Z, Bian Y, Xia T, Zhang L, Chen C. An optimization approach for fabricating electrospun nanofiber air filters with minimized pressure drop for indoor $PM_{2.5}$ control. Build Environ 2021;188:107449.
[16] Schwotzer F, Horak J, Senkovska I, Schade E, Gorelik TE, Wollmann P, et al. Cooperative assembly of 2D-MOF nanoplatelets into hierarchical carpets and tubular superstructures for advanced air filtration. Angew Chem Int Ed 2022;61(22):e202117730.
[17] Liu J, Tian E, Zhang S, Kong D, Liu K, Bai X, et al. The rise of two-dimensional-material-based filters for airborne particulate matter removal. Adv Fiber Mater 2023;5(2):461–83.
[18] Mo J, Zhang Y, Yang R. Novel insight into VOC removal performance of photocatalytic oxidation reactors. Indoor Air 2005;15(4):291–300.
[19] Fan Y, Liu J, Zhao L, Wang C, Moon D, Song S. Study on the test accuracy of the high-air-volume purifier under different test chamber volumes. J Clean Prod 2024;448:141684.
[20] Chen Q, Tian E, Luo Z, Mo J. Adsorption film with sub-milli-interface morphologies via direct ink writing for indoor formaldehyde removal. J Hazard Mater 2022;427:128190.
[21] Chaparro-Garnica CY, Jordá-Faus P, Bailón-García E, Ocampo-Pérez R, Aguilar-Madera CG, Davó-Quiñonero A, et al. Customizable heterogeneous catalysts: nonchanneled advanced monolithic supports manufactured by 3D-printing for improved active phase coating performance. ACS Appl Mater Interfaces 2020;12(49):54573–84.
[22] Chen Q, Chen Z, Wang Y, Tian E, Mo J. Hierarchical diffusion pathways into VOC adsorption films by direct ink writing and ammonium carbonate treatment. Chem Eng J 2023;471:144560.
[23] Liu Y, Cui J, Jiang YX, Li WZ. A numerical study on heat transfer performance of microchannels with different surface microstructures. Appl Therm Eng 2011;31(5):921–31.
[24] Peng P, Gao X, Yan Z, Mintova S. Diffusion and catalyst efficiency in hierarchical zeolite catalysts. Natl Sci Rev 2020;7(11):1726–42.
[25] Zhang Q, Zhou M, Ren G, Li Y, Li Y, Du X. Highly efficient electrosynthesis of hydrogen peroxide on a superhydrophobic three-phase interface by natural air diffusion. Nat Commun 2020;11(1):1731.
[26] Sommer MR, Schaffner M, Carnelli D, Studart AR. 3D printing of hierarchical silk fibroin structures. ACS Appl Mater Interfaces 2016;8(50):34677–85.
[27] Zhou X, Liu C. Three-dimensional printing of porous carbon structures with tailorable pore sizes. Catal Today 2020;347:2–9.
[28] Xia F, Chen Z, Gao Y, Tian E, Mo J. Simultaneous capture and inactivation of airborne bacteria by a dual-zone electrostatically actuated filter. ACS EST Eng 2024;4(4):987–94.
[29] Ji X, Huang J, Teng L, Li S, Li X, Cai W, et al. Advances in particulate matter filtration: materials, performance, and application. Green Energy Environ 2023;8(3):673–97.
[30] Tian E, Gao Y, Mo J. Experimental studies on electrostatic-force strengthened particulate matter filtration for built environments: progress and perspectives. Build Environ 2023;228:109782.
[31] Gao Y, Tian E, Zhang Y, Mo J. Utilizing electrostatic effect in fibrous filters for efficient airborne particles removal: principles, fabrication, and material properties. Appl Mater Today 2022;26:101369.
[32] Thakur R, Das D, Das A. Electret air filters. Sep Purif Rev 2013;42(2):87–129.
[33] Makino H, Emi H, Yamaguchi A, Iritani E, Namiki N. Environmental and safety issues with nanoparticles. In: Naito M, Yokoyama T, Hosokawa K, Nogi K, editors. Nanoparticle technology handbook. Amsterdam: Elsevier; 2018. p. 365–95.
[34] Tian E, Xia F, Wu J, Zhang Y, Li J, Wang H, et al. Electrostatic air filtration by multifunctional dielectric heterocaking filters with ultralow pressure drop. ACS Appl Mater Interfaces 2020;12(26):29383–92.
[35] Cai R, Zhang L. Progress and perspective of polymer electret-based $PM_{2.5}$ filtration: efficiencies, regeneration, and energy implications. Energy 2023;283:128504.

[36] Wang L, Bian Y, Lim CK, Niu Z, Lee PKH, Chen C, et al. Tribo-charge enhanced hybrid air filter masks for efficient particulate matter capture with greatly extended service life. Nano Energy 2021;85:106015.
[37] Li CX, Kuang SY, Chen YH, Wang ZL, Li CJ, Zhu G. In situ active poling of nanofiber networks for gigantically enhanced particulate filtration. ACS Appl Mater Interfaces 2018;10(29):24332–32438.
[38] Park JH, Yoon KY, Hwang JH. Removal of submicron particles using a carbon fiber ionizer-assisted medium air filter in a heating, ventilation, and air-conditioning (HVAC) system. Build Environ 2011;46(8):1699–708.
[39] Wang CS. Electrostatic forces in fibrous filters—a review. Powder Technol 2001;118(1–2):166–70.
[40] Choi DY, Jung SH, Song DK, An EJ, Park D, Kim TO, et al. Al-coated conductive fibrous filter with low pressure drop for efficient electrostatic capture of ultrafine particulate pollutants. ACS Appl Mater Interfaces 2017;9(19):16495–504.
[41] Feng Z, Cao S, Long Z. Determining V-I characteristics of energy-efficient electrostatic assisted air filtration system by utilizing the back-corona induced current model. Energy Built Environ 2023;4(2):227–35.
[42] Zhang G, Zhu Q, Zhang L, Yong F, Zhang Z, Wang S, et al. High-performance particulate matter including nanoscale particle removal by a self-powered air filter. Nat Commun 2020;11(1):1653.
[43] Mo J, Zhang C, Lu Y, Liu Y, Zhang N, Wang S, et al. Radial piston triboelectric nanogenerator-enhanced cellulose fiber air filter for self-powered particulate matter removal. Nano Energy 2020;78:105357.
[44] Jung S, Kim J. Advanced design of fiber-based particulate filters: materials, morphology, and construction of fibrous assembly. Polymers 2020;12(8):1714.
[45] Tian E, Mo J. Toward energy saving and high efficiency through an optimized use of a PET coarse filter: the development of a new electrostatically assisted air filter. Energy Build 2019;186:276–83.
[46] Tian E, Yu Q, Gao Y, Wang H, Wang C, Zhang Y, et al. Ultralow resistance two-stage electrostatically assisted air filtration by polydopamine coated PET coarse filter. Small 2021;17(33):2102051.
[47] Mo J, Gu Y, Tian E. Efficiently remove submicron particles by a novel foldable electrostatically assisted air coarse filter. Sep Purif Technol 2022;288:120631.
[48] Gao Y, Gu Y, Tian E, Mo J. A two-stage cascaded ionizer for boosting PM charging in electrostatic filtration: principles, design, and long-term performance. Sep Purif Technol 2023;313:123494.
[49] Gu Y, Tian E, Xia F, Yu T, Afshari A, Mo J. A new pin-to-plate corona discharger with clean air protection for particulate matter removal. Energy Built Environ 2020;1(1):87–92.
[50] Tian E, Mo J, Long Z, Luo H, Zhang Y. Experimental study of a compact electrostatically assisted air coarse filter for efficient particle removal: synergistic particle charging and filter polarizing. Build Environ 2018;135:153–61.
[51] Gao Y, Tian E, Mo J. Electrically responsive coarse filters endowed by high-dielectric-constant surface coatings toward efficient removal of ultrafine particles and ozone. ACS EST Eng 2021;1(10):1449–59.
[52] Dong W, Gao Q, Zhou S, Tang G, Xiang T, Chun T, et al. Ultra-superhydrophobic MOFs coated on polydopamine-modified polyethylene terephthalate for efficient removal of particulate matter. Chem Eng J 2023;466:143083.
[53] Gao Y, Tian E, Mo J. Electrostatic polydopamine-interface-mediated (e-PIM) filters with tuned surface topography and electrical properties for efficient particle capture and ozone removal. J Hazard Mater 2023;441:129821.
[54] Tian E, Mo J, Li X. Electrostatically assisted metal foam coarse filter with small pressure drop for efficient removal of fine particles: effect of filter medium. Build Environ 2018;144:419–26.
[55] Tian E, Gao Y, Mo J. Electrostatically assisted air coarse filtration for energy efficient ambient particles removal: long-term performance in real environment and influencing factors. Build Environ 2019;164:106348.
[56] Tian E, Liu J, Gao Y, Mo J, Zhang S, Bai X, et al. Artificial polydopamine interface for high-performance ambient particulate matter removal at large velocity. Carbon Neutral 2023;2(2):245–57.
[57] Xia F, Gao Y, Tian E, Afshari A, Mo J. Fast fabricating cross-linked nanofibers into flameproof metal foam by air-drawn electrospinning for electrostatically assisted particle removal. Sep Purif Technol 2021;274:119076.
[58] Hartmann A, Kriegel M. The influence of air ions on the particle concentration in indoor environments—a systematic literature review. Resul Eng 2022;15:100528.
[59] Zhu G, Wang C, Yang T, Gao N, Zhang Y, Zhu J, et al. Bio-inspired gradient poly (lactic acid) nanofibers for active capturing of $PM_{0.3}$ and real-time respiratory monitoring. J Hazard Mater 2024;474:134781.
[60] Yang M, Li X, Yao N, Yu J, Yin X, Zhang S, et al. Two-dimensional piezoelectric nanofibrous webs by self-polarized assembly for high-performance $PM_{0.3}$ filtration. ACS Nano 2024;18(26):16895–904.
[61] Luengas A, Barona A, Hort C, Gallastegui G, Platel V, Elias A. A review of indoor air treatment technologies. Rev Environ Sci Bio 2015;14(3):499–522.
[62] Chen Z, Chen Q, Xu Y, Mo J. Partitioning characteristics of indoor VOCs on impermeable surfaces covered by film-phase DnBP and DEHP. J Hazard Mater Adv 2022;8:100191.
[63] Chen Z, Tian E, Mo J. Removal of gaseous DiBP and DnBP by ionizer-assisted filtration with an external electrostatic field. Environ Pollut 2020;267:115591.
[64] Miao L, Wang JL, Zhang PY. Review on manganese dioxide for catalytic oxidation of airborne formaldehyde. Appl Surf Sci 2019;466:441–53.
[65] Scordo G, Bertana V, Ballesio A, Carcione R, Marasso SL, Cocuzza M, et al. Effect of volatile organic compounds adsorption on 3D-printed PEGDA: PEDOT for long-term monitoring devices. Nanomaterials 2021;11(1):94.
[66] Hasan FA, Xiao P, Singh RK, Webley PA. Zeolite monoliths with hierarchical designed pore network structure: synthesis and performance. Chem Eng J 2013;223:48–58.
[67] Chen Z, Gao Y, Xia F, Afshari A, Mo J. Formation kinetics of SVOC organic films and their impact on child exposure in indoor environments. Sci Total Environ 2024;912:168970.
[68] Liu S, Cheng Z, Li Y, Sun J, Cai K, Huang S, et al. Improved catalytic performance in dimethyl ether carbonylation over hierarchical mordenite by enhancing mass transfer. Ind Eng Chem Res 2020;59(31):13861–21389.
[69] Anand B, Kim KH, Sonwani RK, Szulejko JE, Heynderickx PM. Removal of gaseous benzene by a fixed-bed system packed with a highly porous metal–organic framework (MOF-199) coated glass beads. Environ Res 2022;208:112655.
[70] Liu C, Li Q, Kang W, Lei W, Wang X, Lu C, et al. Structural design and mechanism analysis of hierarchical porous carbon fibers for advanced energy and environmental applications. J Mater Chem A 2022;10(1):10–49.
[71] Chen H, Guo Y, Du Y, Xu X, Su C, Zeng Z, et al. The synergistic effects of surface functional groups and pore sizes on CO_2 adsorption by GCMC and DFT simulations. Chem Eng J 2021;415:128824.
[72] Yang Y, Liu S. Estimation and modeling of pressure-dependent gas diffusion coefficient for coal: a fractal theory-based approach. Fuel 2019;253:588–606.
[73] Lawson S, Adebayo B, Robinson C, Al-Naddaf Q, Rownaghi AA, Rezaei F. The effects of cell density and intrinsic porosity on structural properties and adsorption kinetics in 3D-printed zeolite monoliths. Chem Eng Sci 2020;218:115564.
[74] Wang Y, Liu H, Mei D, Yu S. Direct ink writing of 3D SiC scaffold as catalyst support for thermally autonomous methanol steam reforming microreactor. Renew Energy 2022;187:923–32.
[75] Chen Q, Tian E, Wang Y, Mo J, Xu G, Zhu M. Recent progress and perspectives of direct ink writing applications for mass transfer enhancement in gas-phase adsorption and catalysis. Small Methods 2023;7:2201302.
[76] Ji Q, Luo G, Shi M, Zou R, Fang C, Xu Y, et al. Acceleration of the reaction of H_2S and SO_2 by non-thermal plasma to improve the mercury adsorption performance of activated carbon. Chem Eng J 2021;423:130144.
[77] Zhang J, Duan Y, Zhou Q, Zhu C, She M, Ding W. Adsorptive removal of gas-phase mercury by oxygen non-thermal plasma modified activated carbon. Chem Eng J 2016;294:281–9.
[78] Zhang B, Xu P, Qiu Y, Yu Q, Ma JJ, Wu H, et al. Increasing oxygen functional groups of activated carbon with non-thermal plasma to enhance mercury removal efficiency for flue gases. Chem Eng J 2015;263:1–8.
[79] Pereira A, Ferreira AFP, Rodrigues A, Ribeiro AM, Regufe MJ. Shaping of ZIF-8 and MIL-53(Al) adsorbents for CH_4/N_2 separation. Micropor Mesopor Mater 2022;331:111648.
[80] Lewis JA. Direct ink writing of 3D functional materials. Adv Funct Mater 2006;16(17):2193–204.
[81] Corker A, Ng HC, Poole RJ, Garcia-Tunon E. 3D printing with 2D colloids: designing rheology protocols to predict 'printability' of soft-materials. Soft Matter 2019;15(6):1444–56.
[82] Yuk H, Lu B, Lin S, Qu K, Xu J, Luo J, et al. 3D printing of conducting polymers. Nat Commun 2020;11(1):1604.
[83] Park T, Kara K, Kim D. Flow structure and heat transfer of a sweeping jet impinging on a flat wall. Int J Heat Mass Transf 2018;124:920–8.
[84] Huang K, Elsayed H, Franchin G, Colombo P. 3D printing of polymer-derived SiOC with hierarchical and tunable porosity. Addit Manuf 2020;36:101549.
[85] Liu H, Wei K, Long C. Enhancing adsorption capacities of low-concentration VOCs under humid conditions using NaY@meso-SiO_2 core–shell composite. Chem Eng J 2022;442:136108.
[86] Lawson S, Griffin C, Rapp K, Rownaghi AA, Rezaei F. Amine-functionalized MIL-101 monoliths for CO_2 removal from enclosed environments. Energy Fuels 2019;33(3):2399–407.
[87] Medina DAV, Figuerola A, Rodriguez F, Santos-Neto ÁJ, Cabello CP, Palomino GT, et al. Hyperporous carbon-coated 3D printed devices. Appl Mater Today 2019;14:29–34.
[88] Pellejero I, Almazán F, Lafuente M, Urbiztondo MA, Drobek M, Bechelany M, et al. Functionalization of 3D printed ABS filters with MOF for toxic gas removal. J Ind Eng Chem 2020;89:194–203.
[89] Wang Y, Chen Z, Chen Q, Tian E, Han N, Mo J. Preconcentrating sensor systems toward indoor low-concentration VOC detection by goal-oriented, sequential, inverse design strategy. Build Environ 2024;254:111372.
[90] Le VCT, Sheraz M, Kang E, Ly HN, Mai HD, Anus A, et al. Alumina beads decorated copper-based coordination polymer particle filter for commercial indoor air cleaner. Build Environ 2022;217:109012.
[91] Wu L, Zhang L, Meng T, Yu F, Chen J, Ma J. Facile synthesis of 3D amino-functional graphene–sponge composites decorated by graphene nanodots with enhanced removal of indoor formaldehyde. Aerosol Air Qual Res 2015;15(3):1028–34.
[92] Couck S, Lefevere J, Mullens S, Protasova L, Meynen V, Desmet G, et al. CO_2, CH_4 and N_2 separation with a 3DFD-printed ZSM-5 monolith. Chem Eng J 2017;308:719–26.
[93] Lee KM, Kim NS, Numan M, Kim JC, Cho HS, Cho K, et al. Postsynthetic modification of zeolite internal surface for sustainable capture of volatile

organic compounds under humid conditions. ACS Appl Mater Interfaces 2021;13(45):53925–34.
[94] Vikrant K, Cho M, Khan A, Kim KH, Ahn WS, Kwon EE. Adsorption properties of advanced functional materials against gaseous formaldehyde. Environ Res 2019;178:108672.
[95] Lei B, Liu B, Zhang H, Yan L, Xie H, Zhou G. CuO-modified activated carbon for the improvement of toluene removal in air. J Environ Sci 2020;88:122–32.
[96] Wee J, Bae Y, Ahn H, Choi YO, Jeong E, Yeo SY. Fibrous and granular activated carbon mixed media for effective gas removal as a cabin air filter. Carbon Lett 2022;32(4):1111–8.
[97] Zhang R, Li Z, Zeng L, Wang F. Pressure drop in honeycomb adsorption filters filled with granular activated carbon. Powder Technol 2021;393:550–8.
[98] Zhang Y, Zhu Z, Wang W, Chen S. Mitigating the relative humidity effects on the simultaneous removal of VOCs and $PM_{2.5}$ of a metal–organic framework coated electret filter. Sep Purif Technol 2022;285:120309.
[99] Chen Q, Xiao R, Lei X, Yu T, Mo J. Experimental and modeling investigations on the adsorption behaviors of indoor volatile organic compounds in an *in-situ* thermally regenerated adsorption-board module. Build Environ 2021;203:108065.
[100] Chen Q, Liu F, Mo J. Vertical macro-channel modification of a flexible adsorption board with *in-situ* thermal regeneration for indoor gas purification to increase effective adsorption capacity. Environ Res 2021;192:110218.
[101] Xu Q, Zhang Y, Mo J, Li X. Indoor formaldehyde removal by thermal catalyst: kinetic characteristics, key parameters, and temperature influence. Environ Sci Technol 2011;45(13):5754–60.
[102] Chen Z, Chen Q, Wang Y, Zou W, Li Y, Mo J. Tuning multi-scale pore structures in carbonaceous films via direct ink writing and sacrificial templates for efficient indoor formaldehyde removal. J Hazard Mater 2025;487:137203.
[103] Choma J, Jagiello J, Jaroniec M. Assessing the contribution of micropores and mesopores from nitrogen adsorption on nanoporous carbons: application to pore size analysis. Carbon 2021;183:150–7.
[104] Liu YY, Peyravi A, Dong XB, Hashisho Z, Zheng SL, Chen X, et al. Effect of microstructure in mesoporous adsorbents on the adsorption of low concentrations of VOCs: an experimental and simulation study. J Hazard Mater 2023;458:131934.
[105] Woellner M, Hausdorf S, Klein N, Mueller P, Smith MW, Kaskel S. Adsorption and detection of hazardous trace gases by metal–organic frameworks. Adv Mater 2018;30(37):1704679.
[106] Yang H, Zou Y, Cui H. Advancements and challenges in enhancing salt hydrate phase change materials for building energy storage: optimization methodologies and mechanisms. Natl Sci Open 2024;3(3):20230056.
[107] Flagiello D, Tammaro D, Erto A, Maffettone PL, Lancia A, Di Natale F. Foamed structured packing for mass-transfer equipment produced by an innovative 3D printing technology. Chem Eng Sci 2022;260:117853.
[108] Huang S, Fu H, Wen L. Performance enhancement analysis of a liquid desiccant dehumidifier with internal cooling for indoor benzene removal. Appl Therm Eng 2024;243:122552.
[109] Wang M, Xiao J, Li N, Xu Q, Li H, Chen D, et al. Surface engineering of ternary mixed transition metal oxides for highly efficient catalytic oxidation of low concentration VOCs. Sep Purif Technol 2024;334:126000.